



**Providing Choice & Value**

Generic CT and MRI Contrast Agents



**FRESENIUS  
KABI**

**CONTACT REP**

**AJNR**






This information is current as  
of July 21, 2025.

**MR Cranial Bone Imaging: Evaluation of  
Both Motion-Corrected and Automated Deep  
Learning Pseudo-CT Estimated MR Images**

Andrew D. Linkugel, Tongyao Wang, Parna Eshraghi  
Borojeni, Cihat Eldeniz, Yasheng Chen, Gary B. Skolnick,  
Paul K. Commean, Corinne M. Merrill, Jennifer M. Strahle,  
Manu S. Goyal, Hongyu An and Kamlesh B. Patel

*AJNR Am J Neuroradiol* published online 11 July 2024  
<http://www.ajnr.org/content/early/2024/07/11/ajnr.A8335>

# MR Cranial Bone Imaging: Evaluation of Both Motion-Corrected and Automated Deep Learning Pseudo-CT Estimated MR Images

 Andrew D. Linkugel, Tongyao Wang, Parna Eshraghi Boroojeni,  Cihat Eldeniz, Yasheng Chen,  Gary B. Skolnick, Paul K. Commean,  Corinne M. Merrill, Jennifer M. Strahle,  Manu S. Goyal, Hongyu An, and Kamlesh B. Patel

## ABSTRACT

**BACKGROUND AND PURPOSE:** CT imaging exposes patients to ionizing radiation. MR imaging is radiation free but previously has not been able to produce diagnostic-quality images of bone on a timeline suitable for clinical use. We developed automated motion correction and use deep learning to generate pseudo-CT images from MR images. We aim to evaluate whether motion-corrected pseudo-CT produces cranial images that have potential to be acceptable for clinical use.

**MATERIALS AND METHODS:** Patients younger than age 18 who underwent CT imaging of the head for either trauma or evaluation of cranial suture patency were recruited. Subjects underwent a 5-minute golden-angle stack-of-stars radial volumetric interpolated breath-hold MR image. Motion correction was applied to the MR imaging followed by a deep learning-based method to generate pseudo-CT images. CT and pseudo-CT images were evaluated and, based on indication for imaging, either presence of skull fracture or cranial suture patency was first recorded while viewing the MR imaging–based pseudo-CT and then recorded while viewing the clinical CT.

**RESULTS:** A total of 12 patients underwent CT and MR imaging to evaluate suture patency, and 60 patients underwent CT and MR imaging for evaluation of head trauma. For cranial suture patency, pseudo-CT had 100% specificity and 100% sensitivity for the identification of suture closure. For identification of skull fractures, pseudo-CT had 100% specificity and 90% sensitivity.

**CONCLUSIONS:** Our early results show that automated motion-corrected and deep learning–generated pseudo-CT images of the pediatric skull have potential for clinical use and offer a high level of diagnostic accuracy when compared with standard CT scans.

**ABBREVIATIONS:** AO = AO Foundation; BB = black bone; GA-VIBE = golden-angle stack-of-stars radial volumetric interpolated breath-hold examination; GRE = gradient-echo; ResUNet = residual U-Net; UTE = ultrashort echo; ZTE = zero-echo time

CT quickly generates high-resolution clinical images and has become an indispensable tool for the evaluation of head trauma and craniofacial surgical planning. Approximately 2.2 million CT scans of the head are performed annually on patients younger than 15 years old in the United States.<sup>1</sup> All CT imaging

exposes patients to ionizing radiation, and these 2.2 million head CT scans might result in an estimated 1210 additional future cases of cancer each year.<sup>1</sup> MR imaging can also produce high-resolution images with no exposure to ionizing radiation. However, MR imaging generally involves a longer duration of imaging, sensitivity to motion, and susceptibility to artifacts.<sup>2</sup> Commonly used MR imaging protocols provide superior soft-tissue image quality but limited bone image quality.

The limitation of MR for imaging bone has been a persistent problem since the technique was developed in the 1970s.<sup>3</sup> The gradient-echo black bone MR imaging sequence, first published in 2012,<sup>4</sup> was an initial attempt to address shortcomings of MR imaging for bone imaging. This technique has not achieved widespread clinical use in head trauma due to low sensitivity for the diagnosis of skull fracture,<sup>5</sup> though there has been a promising report for use in craniosynostosis.<sup>6</sup> Specific disadvantages for its use in the pediatric population include sensitivity to motion, poor image contrast between osseous tissue and the surrounding soft tissues, and time-consuming and subjective manual image

Received October 17, 2023; accepted after revision April 19, 2024.

From the Division of Plastic and Reconstructive Surgery (A.D.L., G.B.S., C.M.M., K.B.P.), Mallinckrodt Institute of Radiology (T.W., P.E.B., C.E., P.K.C., M.S.G., H.A.), and Departments of Neurology (Y.C., H.A.), and Neurosurgery (J.M.S.), Washington University in St. Louis, St. Louis, Missouri.

A.D.L. and T.W. contributed equally to this work.

This research was supported by the following Washington University Institute of Clinical and Translational Sciences grants: UL1 TR000448, the Mallinckrodt Institute of Radiology, and the National Institute of Biomedical Imaging and Bioengineering of the National Institutes of Health under Award No. R01EB032713. The content is solely the responsibility of the authors and does not necessarily represent the official views of the National Institutes of Health.

Please address correspondence to Kamlesh B. Patel, MD, MSc, Division of Plastic and Reconstructive Surgery, Washington University in St. Louis, 660 South Euclid Ave, Campus Box 8238, St. Louis, MO 63110; e-mail: kamlesh.patel@wustl.edu

<http://dx.doi.org/10.3174/ajnr.A8335>

## SUMMARY

**PREVIOUS LITERATURE:** There have been several attempts to develop MR imaging sequences for imaging bone, but none have achieved widespread clinical use. Specific challenges include long image acquisition time relative to CT, sensitivity to motion, and requirement for manual image processing to generate useful clinical images. Prior work by our group to develop a golden-angle stack-of-stars radial volumetric interpolated breath-hold examination (GA-VIBE) MR imaging sequence with automated processing by using a deep learning–based technique has shown the potential to ameliorate these issues.

**KEY FINDINGS:** The addition of self-navigated MR motion correction to the prior GA-VIBE sequence and refinement of the residual U-Net (ResUNet) deep learning method has produced cranial images in 72 pediatric patients with high sensitivity and specificity for trauma and suture patency evaluation.

**KNOWLEDGE ADVANCEMENT:** This work represents a significant step toward the goal of using MR imaging to evaluate bone in pediatric patients as part of clinical workflows. We have also identified additional targets for improvement in our image acquisition and processing techniques.

processing. The golden-angle stack-of-stars radial volumetric interpolated breath-hold examination (GA-VIBE) MR imaging sequence, which was originally developed for rapid abdominal imaging, is more robust to motion compared with the gradient-echo black bone MR imaging.<sup>4</sup> We adopted this sequence and demonstrated its feasibility in MR cranial bone imaging.<sup>7,8</sup> However, a subset of scans in previous studies was excluded from clinical review due to excessive motion artifacts. Moreover, a time-consuming manual image processing ranging from 30 minutes to 2 hours imposes difficulty in clinical adoption. Recently, motion correction and deep learning–based techniques were developed to transform MR imaging to pseudo-CT images automatically.<sup>9,10</sup> These prior publications focused on technical developments but have not yet included objective reviews for clinical diagnosis and utility. In this study, we applied both techniques to the GA-VIBE MR images to generate motion-corrected pseudo-CT images. We sought to determine whether the motion-corrected pseudo-CT MR images produce diagnostic quality images for patients presenting after head trauma or for evaluation for craniosynostosis.

## METHODS

### Study Design

Patients were recruited after institutional review board approval was obtained. Patients younger than age 18 who underwent a CT scan of the head as part of routine clinical care for either head trauma or cranial suture patency were invited to participate, and informed consent was obtained from their guardian before participation. Enrolled patients underwent a 5-minute research MR imaging, either as an add-on sequence to a clinically indicated MR imaging (with or without sedation) or a stand-alone research study (no sedation). Sedation was only used in patients who were simultaneously undergoing a clinical MR imaging and the research MR imaging. To mitigate the effects of growth and healing between the clinical and research scans, the research scan was performed as soon as possible, and the MR imaging up to a designated timeframe after the clinical CT scan was allowed to increase scheduling flexibility. For patients with head trauma and at least 1 skull fracture, the research MR imaging was performed up to 12 weeks after their CT. For patients with head trauma and no

skull fracture, the research MR imaging was performed up to 6 months. For patients undergoing evaluation of cranial suture patency, the MR imaging was performed up to 1 year after their CT. Patient demographic data, including age, sex, brief clinical history, the time interval between CT and MR imaging, type of MR imaging scanner, and use of sedation for the clinical scan(s), were collected from the medical record.

### Imaging

The research MR images were acquired by using a Prisma, Vida, or Biograph mMR scanner (Siemens). A FLASH Golden-Angle 3D stack-of-stars radial VIBE sequence<sup>11</sup> was used for radial and Cartesian *k*-space sampling along the in-plane and section directions, respectively. The imaging protocol was as follows: TE/TR = 2.47 ms/4.84 ms; bandwidth = 410 Hz/pixel; section thickness = 0.8 mm; 224 slices per slab; transverse orientation; flip angle = 3–5°; acquisition matrix = 320 × 320; FOV = 192 or 220 mm (depending on head size), resulting in an in-plane resolution of 0.6 × 0.6 mm or 0.7 × 0.7 mm, respectively; and number of radial lines = 400 for a scan duration of about 5 minutes. During each scan, either a 64-channel, a 32-channel, or a 20-channel head coil was used to acquire images.

A self-navigated MR motion correction method has been developed.<sup>9</sup> A brief description is provided below. The section showing the largest intensity variation over time was chosen for its sensitivity to motion, and its temporal signal was used for motion detection. This temporal signal was filtered to remove acquisition-related artifacts and was then parsed into different motion frames by detecting the instances of motion. All frames were registered onto a reference motion frame to obtain motion fields. These motion fields were then used in a forward-modeled iterative optimization scheme to obtain the motion-corrected MR image.

A preliminary version of a deep learning method was developed to convert MR imaging to pseudo-CT by using 3 residual U-Net (ResUNet) models.<sup>10</sup> In this study, a refined approach by using a single ResUNet method was developed. CT images were first trilinearly interpolated to 0.3 × 0.3 × 0.5 mm<sup>3</sup>, followed by a K-means bone, soft tissue, and air segmentation (Matlab R2021b, Mathworks). An edge-enhanced 3 × 3 2D kernel was applied to CT to increase bone and soft tissue contrast. The N4 bias-field

correction was applied to minimize MR imaging spatial inhomogeneity. Level-set segmentation was applied to CT and MR to generate binary head masks. For each subject, MR was aligned to CT by using the FMRIB Linear Image Registration Tool 12-parameter affine registration (FLIRT; <https://fsl.fmrib.ox.ac.uk/fsl/fslwiki/FLIRT>) with 10 times weights in cranial bone alignment between MR and CT.

A 3D patch-based ResUNet was employed to synthesize pseudo-CT by using MR images.<sup>12</sup> Before the ResUNet training, signal intensity normalizations were performed for both CT and MR images as normalized signal = (signal – mean)/(2 × standard deviation). The mean and standard deviation of the CT signal were obtained from all participants, whereas they were computed from each individual participant's MR imaging.

The ResUNet had 7 layers at both contraction and expanding paths. It consisted of skip connections from the residual block to feed outputs from 1 contraction layer to its counterpart in the expanding path. Corresponding MR and CT patches with a size of  $96 \times 96 \times 96$  voxels were randomly selected within the head mask as training input and target, respectively. The 3D ResUNet was trained by using the Adam optimizer with a batch size of 17. The weights of the network were updated by minimizing L1 loss between pseudo-CT and true CT. The learning rate was initialized at 0.005 and empirically decreased by one-half after every 50,000 iterations. The trained network was applied to  $96 \times 96 \times 96$  MR patches in moving windows with a step size of 24 voxels in each direction. The center  $48 \times 48 \times 48$  voxels of patches were used to synthesize pseudo-CT. Pseudo-CT signal was computed as the mean value of the overlapped patches within a voxel. We employed a 3-fold cross-validation procedure in ResUNet training (57%), validation (10%), and testing (33%). We repeated this procedure 3 times to synthesize pseudo-CT for all data sets. The training and validation processes take approximately 65 hours on an NVIDIA H100 Tensor Core graphics processing unit card. It takes about 2 minutes to generate pseudo-CT images for 1 participant.

### Clinical Evaluation

Three reviewers rated the processed MR imaging (pseudo-CT) and CT scans simultaneously in a consensus review. The reviewers were presented with a brief clinical history, including age and reason for imaging. First, for each patient, section-by-section pseudo-CT images were reviewed by using axial, coronal, and sagittal planes in addition to the 3D surface-rendered images as clinically necessary. Only pseudo-CT images were available to the reviewers for this study. Inverted MR images were not utilized. Images were reviewed by using RadiAnt DICOM viewer software (version 2020.2, Medixant). During the pseudo-CT reviews, the reviewers were blinded to the CT diagnosis. For all pseudo-CT scans, acceptability for clinical use was rated on a 4-point scale (1 = inadequate; 2 = sufficient; 3 = good; 4 = excellent). This rating was based on a holistic, subjective assessment by the reviewers of the usefulness of the available scan for clinical diagnosis. Confidence in diagnosis and no need for a second scan were rated on a 5-point Likert scale (1 = strongly disagree; 2 = disagree; 3 = neither agree nor disagree; 4 = agree; 5 = strongly agree). For evaluation of cranial sutures,

patency of the metopic, sagittal, bilateral coronal, and bilateral lambdoid sutures were recorded, for a total of 6 observations per patient. For evaluation of head trauma, the presence or absence of skull fractures in the cranial vault was noted. Any fractures were classified based on AO Foundation (AO) guidelines.<sup>13</sup> The reviewers worked together to assess the scans by using this workflow. After consensus was reached between the reviewers on the pseudo-CT diagnosis for a patient, the corresponding CT images were reviewed in a similar fashion for the same patient, including subjective assessment and reaching consensus on the diagnosis of suture patency or fracture as applicable. Finally, post-CT review acceptability for clinical use of the pseudo-CT was reassessed and rated on the same 4-point scale. The pseudo-CT was deemed inadequate if suture patency or fracture was misdiagnosed. Simultaneous consensus review was used in our protocol because this mirrors the inter- and intradisciplinary review of scans in the clinical workflow at our institution.

### Statistical Analysis

Reviews were collected and tabulated by using Excel (Microsoft). Excel was also used to calculate the sensitivity and specificity of the pseudo-CT-based clinical diagnosis by using the CT images as the ground truth. Qualitative assessments were compared by using the Fisher exact test in R (Version 4.0.3, R Core Team, 2020) running in RStudio.<sup>14</sup> A 2-sided *P* value < .05 was considered statistically significant.

## RESULTS

A total of 72 patients were recruited and underwent CT and MR imaging: 60 patients with head trauma and 12 patients presenting for evaluation of cranial suture patency. Overall, patients ranged from 6 months to 17.8 years old at the time of the CT scan (mean 10.6 years old). Most patients (67%) were male. The preponderance (89%) of the research MR imaging scans were performed without sedation; the remainder were performed with sedation as an add-on sequence to a sedated clinical MR imaging. All MR imaging scans were performed on 3T scanners. For trauma, MR imaging scans were performed between 4 and 168 days (mean 45 days for all patients with trauma, 29 days for patients with a fracture) after the corresponding CT scans. For suture patency, MR imaging scans were performed between 0 and 302 days (mean 65 days) after the corresponding CT scans (Table 1).

### Qualitative Assessment

Before full review for diagnosis, 56 of 72 (78%) of the MR imaging-generated pseudo-CT scans were deemed "excellent" whereas 1 (1%) was deemed "inadequate" for clinical use. On the 5-point Likert scale (1 = strongly disagree to 5 = strongly agree), reviewers agreed (or strongly agreed) that they were confident in their diagnosis by using the pseudo-CT scan in 69 of 72 (96%) cases. The remaining 3 scans (4%) were rated "3 = neither agree nor disagree" for confidence in diagnosis. Reviewers agreed (or strongly agreed) that the imaging was adequate and there was no need for a second scan on 70 (97%) of the pseudo-CT scans. The reviewers neither agreed nor disagreed that a second scan was needed on the remaining 2 scans (3%).

**Table 1: Patient demographics**

Reason for Scan	Age at MR Imaging (Years)*	Number Male Sex	Days from CT to MR*	Number Unsedated
Trauma ( <i>n</i> = 60)	12.2 ± 4.2	38 (63%)	45 ± 39	58 (97%)
Suture Patency ( <i>n</i> = 12)	2.5 ± 4.2	10 (83%)	65 ± 92	6 (50%)
All ( <i>n</i> = 72)	10.6 ± 5.4	48 (67%)	49 ± 51	64 (89%)

\*Mean ± standard deviation.

**Table 2: Qualitative assessment Likert scales (all patients *n* = 72)**

	Confident in Diagnosis		Need Another Scan	
	Pseudo-CT	CT	Pseudo-CT	CT
Strongly disagree	0	0	58	71
Disagree	0	0	12	1
Neither agree nor disagree	3	0	2	0
Agree	11	1	0	0
Strongly agree	58	71	0	0
<i>P</i> value	.300		.300	

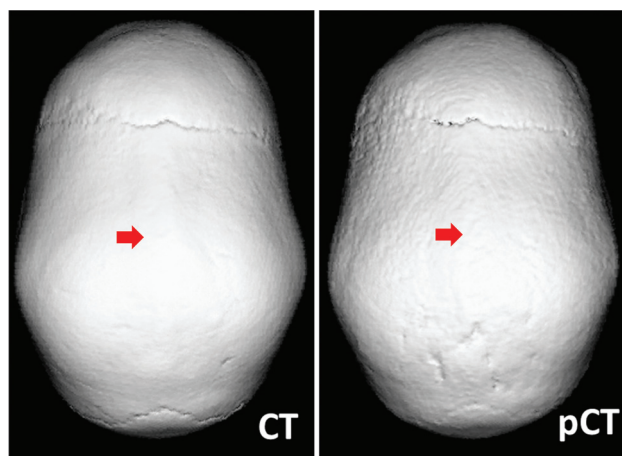


**FIG 1.** Representative CT (*left*) and pseudo-CT (*right*) scans for evaluation of cranial suture patency. Arrows indicate prematurely fused sagittal suture.

In comparison, all 72 (100%) of the CT scans were graded “excellent” for clinical use. For 71 (99%) CT scans, reviewers strongly agreed they were confident in their diagnosis and strongly agreed that there was no need for a second scan on the Likert scale. Differences between techniques did not reach statistical significance in the level of confidence in diagnosis or the need for a second scan; *P* = .300 for both (Table 2).

After both CT and pseudo-CT scans were reviewed, acceptability for clinical use of the pseudo-CT scan was reassessed. At that time, reviewers graded 59 of the 72 (82%) scans as “excellent,” 7 (10%) as “good,” 4 (6%) as “sufficient,” and 2 (3%) as “inadequate.”

### Clinical Diagnosis

For cranial suture patency, a total of 72 sutures were evaluated in 12 patients. The diagnosis was concordant between CT and pseudo-CT for all sutures, with 51 patent, 2 partially fused, and 19 fully fused sutures. Thus, by using the CT as the reference standard, pseudo-CT had 100% specificity and 100% sensitivity for suture closure. Representative CT and pseudo-CT scans of a patient evaluated for suture patency are shown in Fig 1. In the 60 patients evaluated for head trauma, fractures were identified on 9

subjects by using pseudo-CT. With the CT available, an additional fracture was identified in another patient. One patient had multiple fractures. This was correctly noted based on pseudo-CT as well as CT. All fractures were nondisplaced, and the type of fracture was also correctly identified via the pseudo-CT images. In sum, CT and pseudo-CT produced concordant diagnosis in 59 of

60 (98%) patients with head trauma. With CT as the reference standard, pseudo-CT had 100% specificity and 90% sensitivity for diagnosis of skull fracture in patients with pediatric head trauma. Representative pseudo-CT and CT scans for trauma are shown in Fig 2. The patient whose fracture was identified on the CT, but not the pseudo-CT, was 4 years old, and the interval between CT scan and MR imaging was 9 weeks (Fig 3).

### DISCUSSION

The low proton attenuation and short T2\* lead to low signal in cranial bone on conventional MR images. Eley et al<sup>4</sup> proposed a black bone (BB) approach to separate bone from soft tissue by using standard Cartesian gradient-echo (GRE) images. However, it is challenging to separate bone from air in the BB GRE images. Furthermore, the Cartesian *k*-space readout of BB-GRE is sensitive to motion artifacts. More recently, ultrashort echo (UTE) and zero-echo time (ZTE) MR have been explored for cranial bone imaging.<sup>15,16</sup> A subtraction between the first and second echo of the dual-echo UTE have been used to separate bone, soft tissue, and air. Conversely, 2 separate thresholds were used to separate soft tissue and bone and air and bone on logarithmic inverted ZTE. A recent study directly compared BB-GRE, a dual radiofrequency dual-echo UTE, and ZTE in adult cranial bone imaging.<sup>17</sup> Though bone segmentations by 3 methods were comparable, UTE and ZTE showed better bone and air contrasts than GRE. Due to insufficient bias field correction and the 2 signal thresholds used in separating bone from air and soft tissue in ZTE, bone classification was more challenging in ZTE than in UTE. In contrast, the UTE method benefits from the self-normalization in the dual-echo subtraction. However, UTE is not a vendor-provided standard sequence and requires scanner-specific gradient delay corrections.

Thus far, existing BB-GRE and UTE/ZTE methods primarily relied on MR signal intensity to identify skull fractures or sutures by using manual image processing without motion correction.<sup>5,6,18</sup> Dremmen et al<sup>5</sup> reported a sensitivity of 67% and a specificity of 88% in identifying fractures. Kralik et al<sup>18</sup> reported an overall sensitivity of 83% and a specificity of 100% in fracture detection; however, the sensitivity was decreased to 50% in unsedated patients. To the best of our knowledge, our study is

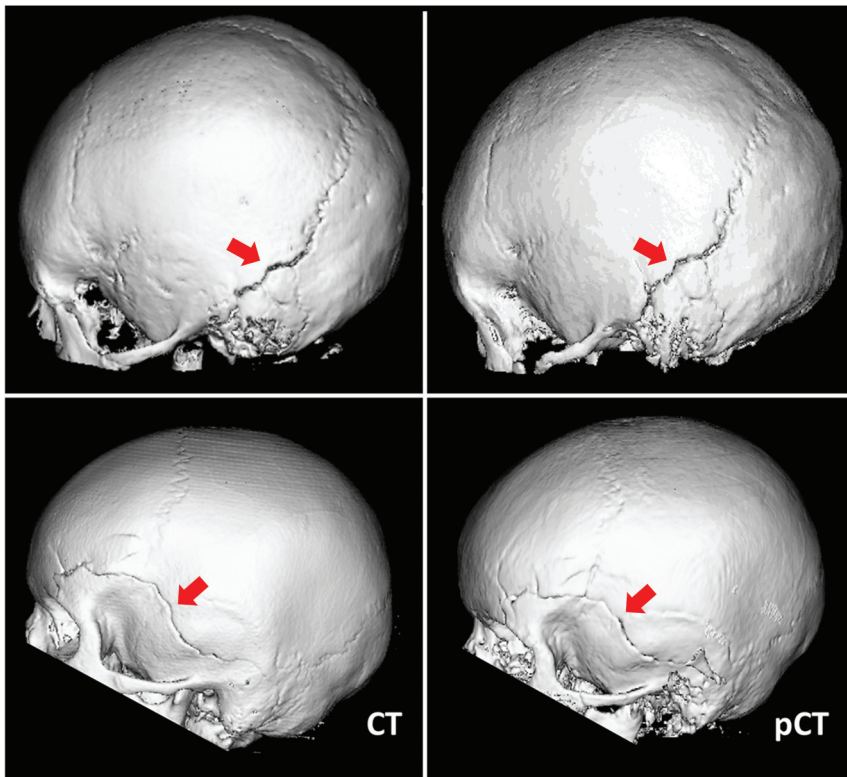


**FIG 2.** Representative CT (*left*) and pseudo-CT (*right*) scans for head trauma in 2 patients. Arrows indicate left occipital bone fracture in the first patient and fracture of the left temporal, parietal, and frontal bones in the second patient.

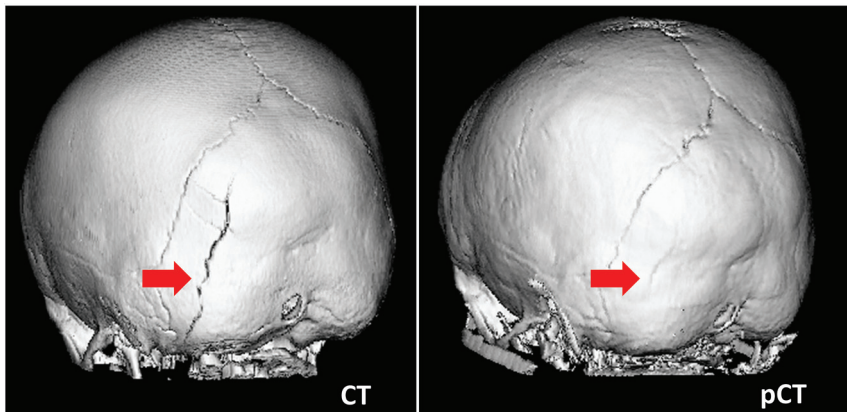


**FIG 3.** Discordant diagnosis of skull fracture. *Left* arrow indicates occipital bone fracture present on CT, with interval healing on pseudo-CT (*right* arrow).

the first study to incorporate both motion correction and deep learning-generated pseudo-CT to evaluate cranial bone imaging in pediatric patients with craniosynostosis and head trauma. The radial VIBE sequence in our study allows self-navigated motion correction. Moreover, ResUNet-generated pseudo-CT overcomes signal overlap issues in threshold-based approaches. Our proposed method reached 100% sensitivity and 100% specificity for cranial suture patency and 90% sensitivity and 100% specificity for fractures. Of note, our deep learning pseudo-CT approach can be extended to convert UTE and ZTE images to pseudo-CT images.

patients. In our initial study design, the relatively high and heterogeneous maximum time intervals between CT and MR imaging scans were used to facilitate patient recruitment. Of note, to increase the number of eligible patients in this pilot study, the suture patency group included some children older than the typical age for primary evaluation of craniosynostosis. In future validation of this technique for suture patency, we aim to narrow the eligibility to patients younger than 1 year of age. In addition, we will restrict MR imaging to within 4 weeks of the CT imaging to avoid further cases of discordant diagnosis. In this study, MR images were acquired from 64-, 32-, and

The MR imaging protocols in this study generated CT-like images of bone from a diverse set of pediatric patients. In 71 of 72 patients, the pseudo-CT led to a concordant diagnosis with the CT scan, and in 96% of the cases, reviewers agreed or strongly agreed that they were confident in the diagnosis. Of the 72 patients imaged in this study, there was a single case of discordant diagnosis between the CT and pseudo-CT. Sedation was not used for this MR imaging. In this case, a 4-year-old patient had no fracture identified on pseudo-CT but had an occipital bone fracture present on the reference-standard CT. These scans were performed 9 weeks apart, again within the inclusion criteria of this study. Pediatric skull fractures show wide variability in time to radiographic healing, ranging from 2 to 18 weeks in 1 study of patients younger than 24 months old with skull fractures.<sup>19</sup> Based on their overall similar appearance and clearly visible lambdoid sutures on both the CT and pseudo-CT, it is reasonable to assume radiographic healing may have occurred in the 9-week interval between the scans in this young patient (Fig 3).

There were other shortcomings identified in the pseudo-CT scans that did not result in discordant diagnosis. In some cases, muscle, such as the temporalis, was rendered similar to bone in the pseudo-CT. In addition, the automated image processing anecdotally performed more poorly in highly aerated areas of the skull with thin overlying bone, such as the frontal and mastoid sinuses. By design, the neural network will improve over time with more exposure to data. A significant limitation in the present study is the time interval between CT and MR imaging for some of the included

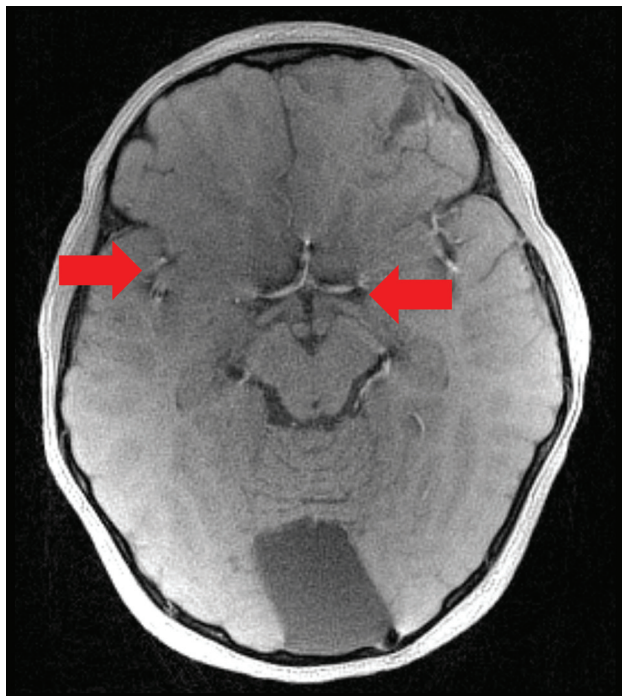


**FIG 4.** Source MR image for patient with fracture, showing brain parenchymal injury and artifact in the basal CSF spaces (arrows).

20-channel head coils. Due to the spatial sensitivity of the coils, the SNR ratio and signal spatial heterogeneity varied greatly in the data. The 20-channel coil images have a much lower SNR than 32- and 64-channel data. Moreover, 64-channel data had more spatial signal heterogeneity with high signal in the cortical region compared with 20- and 32-channel data. Despite these differences, the ResUNet-generated pseudo-CT provides comparable clinical evaluations, suggesting its robustness to various SNR and signal spatial heterogeneity. Future work may further evaluate its performance in data acquired by using different imaging parameters or with a shorter acquisition time.

Though the pseudo-CT images are useful for evaluating cranial bone for fracture and suture patency, the source MR images produced by this sequence are also useful for evaluating any underlying brain parenchymal injury (Fig 4). Artifacts, possibly produced by the vasculature on the source MR images, can be propagated through the pseudo-CT processing, resulting in apparent hyperattenuations in the CSF space. Further study will be necessary to determine which clinical applications are most appropriate for use of MR for cranial bone imaging versus CT cranial bone imaging.

Overall, the pseudo-CT images in this study represent the early evolution of the training process for automated creation of pseudo-CT images from MR imaging scans. It must be emphasized that this MR image is an experimental protocol that requires further improvement and validation before integration into clinical workflows. After continued iterative improvement to the MR images used in this study, final clinical validation will include multicenter studies with real-time MR acquisition and analysis as part of clinical care. If integrated into MR imaging scanners already present in hospitals, an MR imaging protocol with short scan duration, no requirement for sedation, and

reliable automated image processing would have tremendous clinical use for bone imaging in both children and adults. In addition, this technology could be applied to the development of similar protocols for MR imaging of the facial skeleton, another area where CT images are currently vital.

## CONCLUSIONS

GA-VIBE MR cranial images with motion correction and pseudo-CT processing have the potential to replace many of the CT scans performed to evaluate the cranial vault in pediatric patients. Further improvement in scan duration, motion correction, and image processing techniques will continue to advance bone MR imaging toward the ultimate goal of clinical utility.

Disclosure forms provided by the authors are available with the full text and PDF of this article at [www.ajnr.org](http://www.ajnr.org).

## REFERENCES

- Miglioretti DL, Johnson E, Williams A, et al. **The use of computed tomography in pediatrics and the associated radiation exposure and estimated cancer risk.** *JAMA Pediatr* 2013;167:700–07 [CrossRef](#) [Medline](#)
- Davis PC; Expert Panel on Neurologic Imaging. **Head trauma.** *AJNR Am J Neuroradiol* 2007;28:1619–21 [Medline](#)
- Moseley I, Brant-Zawadski M, Mills C. **Nuclear magnetic resonance imaging of the orbit.** *Br J Ophthalmol* 1983;67:333–42 [CrossRef](#) [Medline](#)
- Eley KA, McIntyre AG, Watt-Smith SR, et al. **“Black bone” MRI: a partial flip angle technique for radiation reduction in craniofacial imaging.** *Br J Radiology* 2012;85:272–78 [CrossRef](#) [Medline](#)
- Dremmen MHG, Wagner MW, Bosemani T, et al. **Does the addition of a “black bone” sequence to a fast multisequence trauma MR protocol allow MRI to replace CT after traumatic brain injury in children?** *AJNR Am J Neuroradiol* 2017;38:2187–92 [CrossRef](#) [Medline](#)
- Saarikko A, Mellanen E, Kuusela L, et al. **Comparison of black bone MRI and 3D-CT in the preoperative evaluation of patients with craniosynostosis.** *J Plast Reconstr Aesthet Surg* 2020;73:723–31 [CrossRef](#) [Medline](#)
- Patel KB, Eldeniz C, Skolnick GB, et al. **3D pediatric cranial bone imaging using high-resolution MRI for visualizing cranial sutures: a pilot study.** *J Neurosurg Pediatr* 2020;26:311–17 [CrossRef](#) [Medline](#)
- Patel KB, Eldeniz C, Skolnick GB, et al. **Cranial vault imaging for pediatric head trauma using a radial VIBE MRI sequence.** *J Neurosurg Pediatr* 2022;30:113–18 [CrossRef](#) [Medline](#)
- Eldeniz C, Commean PK, Boroojeni PE, et al. **Motion-corrected radial head MRI without any navigator, data redundancy or external tracking.** Abstract presented at: International Society for Magnetic Resonance in Medicine; May 11, 2022; London, England, United Kingdom. <https://submissions.miramart.com/ISMRM2022/Itinerary/ConferenceMatrixEventDetail.aspx?ses=G-04>
- Eshraghi Boroojeni P, Chen Y, Commean PK, et al. **Deep-learning synthesized pseudo-CT for MR high-resolution pediatric cranial bone imaging (MR-HiPCB).** *Magn Reson Med* 2022;88:2285–97 [CrossRef](#) [Medline](#)
- Peters DC, Korosec FR, Grist TM, et al. **Undersampled projection reconstruction applied to MR angiography.** *Magn Reson Med* 2000;43:91–101 [CrossRef](#)
- Chen Y, Ying C, Binkley MM, et al. **Deep learning-based T1-enhanced selection of linear attenuation coefficients (DL-TESLA) for PET/MR attenuation correction in dementia neuroimaging.** *Magn Reson Med* 2021;86:499–513 [CrossRef](#) [Medline](#)
- Ieva AD, Audigé L, Kellman RM, et al. **The comprehensive AOCMF classification: skull base and cranial vault fractures—level 2 and 3 tutorial.** *Craniofacial Trauma Reconstr* 2014;7:S103–13 [CrossRef](#) [Medline](#)

14. **RStudio: integrated development environment for R.** RStudio Team. <http://www.rstudio.com/> Accessed April 1, 2024
15. Wiesinger F, Sacolick LJ, Menini A, et al. **Zero TE MR bone imaging in the head.** *Magn Reson Med* 2016;75:107–14 [CrossRef Medline](#)
16. Lee H, Zhao X, Song HK, et al. **Rapid dual-RF, dual-echo, 3D ultra-short echo time craniofacial imaging: a feasibility study.** *Magn Reson Med* 2019;81:3007–16 [CrossRef Medline](#)
17. Kamona N, Jones BC, Lee H, et al. **Cranial bone imaging using ultrashort echo-time bone-selective MRI as an alternative to gradient-echo based “black-bone” techniques.** *Magma N MAGMA* 2024;37:83–92 [CrossRef Medline](#)
18. Kralik SF, Supakul N, Wu IC, et al. **Black bone MRI with 3D reconstruction for the detection of skull fractures in children with suspected abusive head trauma.** *Neuroradiology* 2019;61:81–87 [CrossRef Medline](#)
19. Harper NS, Eddleman S, Shukla K, et al. **Radiologic assessment of skull fracture healing in young children.** *Pediatr Emerg Care* 2021;37:213–17 [CrossRef Medline](#)